INTERNATIONAL JOURNAL OF HYDROGEN ENERGY XXX (2018) 1–12

Available online at www.sciencedirect.com

ScienceDirect

journal homepage: www.elsevier.com/locate/he

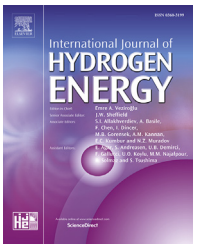

Numerical optimization of channel to land width ratio for PEM fuel cell

Mohammad Ziauddin Chowdhury [a,b,*], *Omer Genc* [a,b], *Serkan Toros* [a,b]

[a] *Nigde Omer Halisdemir University Prof. Dr. T. Nejat Veziroglu Clean Energy Research Center, Nigde, Turkey*
[b] *Mechanical Engineering Department, Faculty of Engineering, Nigde Omer Halisdemir University, Nigde, Turkey*

ARTICLE INFO

Article history:
Received 14 August 2017
Received in revised form
10 December 2017
Accepted 23 December 2017
Available online xxx

Keywords:
Pressure drop
Current density
Channel geometry
Mathematical modeling

ABSTRACT

Flow field plays a vital role in proton exchange membrane (PEM) fuel cell where channel geometry being the primary factor. Most of the channel geometry analyses were limited to few number of case studies, whereas in this study total 73 case studies were analyzed for the optimization of channel and land width. A three dimensional isothermal single phase flow mathematical model is developed and further validated with experimental study to optimize the channel and land width through parametric sweep function for a staggering 73 number of case studies. The optimization analyses are carried out for a straight channel geometry considering a fixed operating voltage of 0.4 V and channel depth of 1.0 mm. Due to the large number of case studies, the analyzed performance parameters i.e. current density and pressure drop are easily understandable for the change in different channel and land width. The numerical results predicted that the pressure drop is more dependent on channel width compare to the land width and anode pressure drop is less significant than cathode pressure drop. However, both channel and land width have an equal importance on the cell current density. Considering channel pressure drop and current density, the optimization analyses showed that the channel to land width of 1.0 mm/1.0 mm would be best suitable for PEMFC channel geometry.

Introduction

Proton exchange membrane (PEM) fuel cell is an emerging sustainable energy source [1] that can fulfill the growing demand especially for automotive sectors [2,3]. For this reason, large scale research interest is on the rise for the efficient PEM fuel cell system development. Bipolar plate is one of the major component in PEM fuel cell contributing 60% weight and 30% cost of the PEM fuel cell system [4]. Ozden et al. [5] numerically investigated that cell degradation is more prone to the bipolar plate than other system components of PEMFC. Bipolar plate facilitates flow fields through which reactants flow, electron conduction and removal of waste heat and water from the cell take place as well. That's why bipolar plate has a great significance on the PEM fuel cell system. The optimization of bipolar plate flow field geometry is very difficult through experimental approach, whereas numerical procedure is an effective tool for the optimization [6–8].

The cell performance of PEM fuel cell largely relies on the proper flow field design. For the effective flow field design, channel geometry is the primary dominant factor. This is because improper channel geometry can results in maldistribution of reactants transport [9,10] faulty water

* *Corresponding author*. Nigde Omer Halisdemir University Prof. Dr. T. Nejat Veziroglu Clean Energy Research Center, Nigde, Turkey.
E-mail addresses: zia72822@gmail.com (M.Z. Chowdhury), omergenc@ohu.edu.tr (O. Genc), serkantoros@ohu.edu.tr (S. Toros).
https://doi.org/10.1016/j.ijhydene.2017.12.149
0360-3199/

Nomenclature

A_c	Tafel slope
E_{eq}	Equilibrium voltage
μ	Dynamic viscosity
a_v	Active surface area
C_x	Species concentration
D_{ik}	Diffusion coefficient
F	Faraday constant
i	Current Density
i_0	Exchange current density
i_v	Total local current density
K	Permeability
M	Molecular mass
P	Pressure
R	Universal gas constant
R_i	Species source term
S	Current source term
T	Cell temperature (K)
u	Velocity
ω	Mass fraction
x	Mole fraction
J_i	Diffusive flux
N_i	Total flux
η	Electrochemical overpotential
ρ	Mixture density
σ	Electric conductivity
φ	Phase potential
α	Charge transfer coefficient
ε	Porosity

Subscript

a	anode
c	cathode
o	initial condition
l	electrolyte phase
s	solid phase
ik	species
ref	reference
eq	equivalent
v	totality

management [11–13] and high pressure drop [10,14] across the flow field active area resulting poor cell performance. In the flow field geometry, channel width/land ratio plays a significant role for the optimized flow field design as well as for better cell performance. There are several studies for the channel width/land ratio optimization with numerical investigation [8,15,16]. The increase of channel width causes better cell performance reducing the concentration loss effectively which leads to an increasing of current density [17]. On the other hand, narrow land width increase ohmic loss by increasing contact resistance between bipolar plate and gas diffusion layer [18]. Yu et al. [19] investigated that the land width has little influence on the improvement of cell performance for interdigitated flow field due to the forced convection gas transfer mechanism. Goebel et al. [20] recommended minimum land fraction of a 50% for low contact resistance with a maximum 1.0 mm channel span. Channel to land width ratio found to be less significant for transient temperature distribution while scale ratio of 1.0 is highly desirable for the power gain function [21]. Pressure drop increases with the decreasing channel size and if pump work is neglected small channel cross-sectional area would be better for cell performance [22].

Understanding the in-situ characteristics of the mass transport phenomena and electrochemical process, numerical technique is becoming more popular approach [23–25] and due to this, reliability is a major concern of the numerical solution of PEMFC. Anderson et al. [26] made comprehensive analyses on flow phase of PEMFC modeling techniques. Finite element method by Comsol multiphysics interface was used for the PEM fuel cell simulation in several studies [27–31]. Hasse et al. [32]. investigated differential pressure using finite element analyses. Verma et al. [33] numerically analyzed membrane properties and water management on PEM fuel cell performance considering two dimensional single phase flow. Ismail et al. [34]. employed a three dimensional single phase flow model to explore the effect of permeability on the gas diffusion layer. Cooper et al. [35] presented a three dimensional single phase flow to investigate the effect of channel aspect ratio on cell performance. To optimize flow field design, single phase flow was considered, explaining the standard working temperature of 80 °C is sufficient enough for gas flow phase to be unchanged especially for isothermal condition [6,8,36,37]. Furthermore, for the small active area, eliminating the liquid water formulation and transport will not be a major issue as the single phase transport can be assumed for the comparative flow fields' study of mass transport concentration, pressure and current density distribution analyses considering steady state isothermal conditions. Ghanbarian et al. [38] explained that single phase module can detect condensing regions using the concentration profile analyses of two phase transport.

So far, there are so many studies being accomplished considering only few number of cases for the channel to land width optimization. In this study, a three dimensional isothermal single phase flow numerical model is considered for the optimization of channel to land width for PEM fuel cell. The most significant aspect of this study is that a total number of 73 cases of channel to land width ratio are analyzed for optimization with the parametric sweep function analyses.

Mathematical model

A mathematical model is developed based on two major consequences of PEMFC, which are the charge phenomena and fluid flow dynamics. Mathematical model consists of the governing equations considering assumptions, initial conditions and boundary conditions, numerical technique, mesh independency test for reliable solution and model validation.

Geometry of interest

The generalized computational 3D domain of the considered cases is shown in Fig. 1, while the considered channel width and land width are listed in Table 1. All the studied cases have

Please cite this article in press as: Chowdhury MZ, et al., Numerical optimization of channel to land width ratio for PEM fuel cell, International Journal of Hydrogen Energy (2018), https://doi.org/10.1016/j.ijhydene.2017.12.149

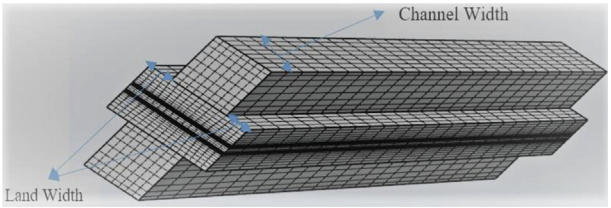

Fig. 1 – Structural mesh of the computational geometry.

the same channel depth of 1.0 mm to understand the PEMFC behavioral change with different channel to land width ratio. The land width is taken in both side of the flow channel as shown in Fig. 1 and geometric dimensions are same for both anode and cathode channel for each case study. Structural meshes are used for all considered case studies as there is no complexity in geometry for the straight channel. The number of mesh elements for each case is decided after a mesh independency test, resulting in almost equal number of mesh elements. The structure is consists of approximately 14,448 domain elements, 5870 boundary elements, and 848 edge elements. For the different channel and land width of the geometry, the mesh is automatically changed with respect to the geometry change. The numerical analysis of this study considered several values for channel width and land width considering all the possible combination of channel and land width listed in Table 1.

Model assumptions

The following assumptions are made for the mathematical model developed in this study [39]:

- Steady state operating conditions
- All gases and gas mixture behavior are considered as ideal gas and gas mixture conditions
- Isothermal model
- Single phase incompressible flow without any phase change
- There is no crossover of reactants and water vapor through electrolyte membrane
- Electrolyte is electrically insulated
- The effect of gravity is neglected
- Fixed gas compositions at the inlets of both the anode and cathode
- Negligible back pressure
- No film resistance for GDL and catalyst layer

Governing equations

The governing equations under the above-mentioned assumptions are described below for electrochemical and fluid dynamics solution of the considered geometric models.

Electrochemical model

The electrochemical model solved the electrode kinetics in anode and cathode considering the linearized Butler-Volmer and cathodic Taefl equations respectively [35]. The electricity is generated as a result of the electrochemical reactions taking place in the anode and cathode electrodes. This electrochemical process is related with the charge production, transport and conservation. Thus, the mathematical model in this study considers the related theories by developing associated governing mathematical equations. In PEMFCs, the bipolar plate rib (land) surface, porous electrodes and membrane are the charge transport mediums, while the porous catalysts are responsible for the charge production. The hydrogen oxidation reaction (HOR) occurs at anode catalyst as follows:

$$H_2 \rightarrow 2H^+ + 2e^- \tag{1}$$

Therefore, local current density for HOR is developed using the linearized concentration depended Butler-Volmer equation [40] can be derived as follows:

$$i_a = (i_{0,ref})_a i_{o,a}\left(\frac{\alpha_{a,a}+\alpha_{c,a}}{RT}F\eta_a\right) \tag{2}$$

where $i_{o,a}$ is the anode exchange current density, $(i_{0,ref})_a$ is the reference anode exchange current density, R is the ideal gas constant, F represents the Faraday constant, T stands for the operation temperature (K) and η_a shows the anode overpotential. $\alpha_{a,a}$ and $\alpha_{c,a}$ is the anodic and cathodic charge transfer constant for the anode, respectively. The anode exchange current density $i_{o,a}$ can be calculated as a function of the local H_2 concentration C_{H_2} and the reference H_2 concentration $C_{H_2,ref}$ as follows [40]:

$$i_{o,a} = \left(\frac{C_{H_2}}{C_{H_2,ref}}\right)^{0.5} \tag{3}$$

Similarly, in the cathode catalyst, the oxygen reduction reaction (ORR) occurs:

$$½O_2 + 2H^+ + 2e^- \rightarrow H_2O \tag{4}$$

The local current density in the cathode for ORR can be expressed using cathodic Tafel equation:

$$i_c = -(i_{0,ref})_c i_{o,c} 10^{\eta_c/A_c} \tag{5}$$

$$i_{o,c} = \left(\frac{C_{O_2}}{C_{O_2,ref}}\right) \tag{6}$$

In the above equation, $i_{o,c}$ represents the cathode exchange current density, $(i_{0,ref})_c$ is the reference cathode exchange current density and C_{O_2} and $C_{O_2,ref}$ is the local and reference O_2 concentration, respectively. A_c represents Tafel slope while η_c is the cathode overpotential.

The potential difference between the solid matrix and the electrolyte for the electrodes is the electrochemical

Table 1 – Considered cases of channel width (mm) and land width (mm).

Channel width	0.2	0.25	0.3	0.4	0.5	0.6	0.7	0.75	0.8	0.9	1	1.1	1.2	1.25	1.3	1.4	1.5	1.75	2
Land width	–	0.25	–	0.4	0.5	0.6	0.7	0.75	0.8	0.9	1	1.1	1.2	1.25	1.3	1.4	1.5	–	–

Please cite this article in press as: Chowdhury MZ, et al., Numerical optimization of channel to land width ratio for PEM fuel cell, International Journal of Hydrogen Energy (2018), https://doi.org/10.1016/j.ijhydene.2017.12.149

overpotential (η) which can be defined as a function of electronic (ϕ_s) and ionic (ϕ_l) phase potential as well as equilibrium voltage (E_{eq}) as:

$$\eta = \phi_s - \phi_l - E_{eq} \tag{7}$$

The continuity of current density (i) can be expressed as:

$$\nabla \cdot i = 0 \tag{8}$$

As in the PEMFC, there are two types of charge, which are electronic (i_s) and ionic (i_l). Then, Eqn. (8) can be rearranged as:

$$\nabla \cdot i_s + \nabla \cdot i_l = 0 \tag{9}$$

Applying Ohm's Law to the charge transfer with the account of electronic (S_s) and ionic (S_l) charge source term, Eqn. (9) becomes [39]:

$$\nabla \cdot (-\sigma_s \nabla \phi_s) = S_s \;\; ; \;\; \nabla \cdot (-\sigma_l \nabla \phi_l) = S_l \tag{10}$$

where σ is the conductivity, subscript's' and 'l' denote to solid and electrolyte phase respectively. Due to the electrochemical reactions in the anode and cathode catalyst layers, the current source terms are linked to the corresponding local two-phase current densities of the anode and cathode, respectively in eqns. (11) and (12), as follows [40]:

$$S_s = -i_a \;\; ; \;\; S_l = i_a \tag{11}$$

$$S_s = -i_c \;\; ; \;\; S_l = i_c \tag{12}$$

The total local current density for the active surface area for the anode and cathode electrode kinetics becomes, respectively:

$$i_{v,a} = a_{v,a} i_a \;\; ; \;\; i_{v,c} = a_{v,c} i_c \tag{13}$$

Therefore, the agglomerated charge module with the account of the charge source terms, the total local current density and charge transport respectively, for both the anode and cathode can be expressed in generalized form, as follows:

$$\nabla \cdot i_s = S_s - i_v \;\; ; \;\; \nabla \cdot i_l = S_l + i_v \tag{14}$$

Fluid dynamics model

The reactant gas flows in the gas channels for both anode and cathode are governed by the continuity equation [41] for the conservation of mass and Navier-Stokes equations [42] describe the momentum conservation of Newtonian fluids. Based on the model assumptions, the final forms of continuity and Navier-Stokes equations are given below, respectively:

$$\nabla \cdot \rho u = 0 \tag{15}$$

$$\rho u \cdot \nabla u = \nabla \cdot \left[-P + \mu \left(\nabla u + \mu (\nabla u)^T \right) - \frac{2}{3} \mu (\nabla \cdot u) \right] \tag{16}$$

where u is the flow velocity, μ is the dynamic viscosity of the gas mixture, ρ shows the gas mixture density, and P is the pressure.

Brinkman equations of extended Navier-Stokes equation is applied for porous layers (GDL and CL) mass and momentum conservation [43] neglecting Forchheimer drag $\mathbf{F}$, due to single phase flow existence as there is no force of fluid body, which are

$$\nabla \cdot (\rho u) = R_i \tag{17}$$

$$\frac{\rho}{\varepsilon} \left((u \cdot \nabla) \frac{u}{\varepsilon} \right) = \nabla \cdot \left[-P + \frac{\mu}{\varepsilon} \left(\nabla u + (\nabla u)^T \right) - \frac{2\mu}{3\varepsilon} (\nabla \cdot u) \right] - \left(\frac{\mu}{K} + R_i \right) u + \mathbf{F} \tag{18}$$

where ε is porosity, permeability K, and source term for mass generation is R_i in GDL is zero.

Species balance in the gas channel and GDL is governed by Ref. [36].

$$\rho \varepsilon \frac{\delta \omega_i}{\delta t} + \nabla \cdot J_i + \rho (u \cdot \nabla) \omega_i = 0 \tag{19}$$

$$N_i = J_i + \rho u \omega_i \tag{20}$$

where J_i and N_i are diffusive flux and total flux of species i.

The multi-component convection and diffusion in the flow channels and GDL are described by the Maxwell-Stefan equation to solve the mass fraction (ω) fluxes. The mathematical form of the Maxwell-Stefan equation is used as [36]:

$$J_i = -\rho \omega_i \sum_k D_{ik} \left[\nabla x_k + \frac{1}{P} (x_k - \omega_k) \nabla P \right] + D_i^T \frac{\nabla T}{T} \tag{21}$$

D_{ik} terms in the Eqn. (17) are the Maxwell-Stefan diffusivities and they are listed in Table 2. The total mass fraction ω_i for anode and cathode individually is as follows:

$$\sum_i \omega_i = 1 \tag{22}$$

The diffusion coefficients in the porous anode and cathode layers needs to be correlated with the porosity of the medium (ε). The effective diffusion coefficients for the anode and cathode layers are corrected as follows [40]:

$$D_{ik}^{eff} = D_{ik} \varepsilon^{1.5} \tag{23}$$

where the diffusion coefficient of specie (i) is a function of temperature and pressure [40], i.e.,

$$D_i = D_{0,i} \left(\frac{T}{T_0} \right)^{1.5} \frac{P_0}{P}$$

The density of mixture gas is a function of mixture components and is described by the following equation:

$$\rho = \left(\sum_i x_i M_i \right) P / (RT) \tag{24}$$

where x_i and M_i is the molar fraction and molecular weight of specie i, respectively.

On the anode side, the hydrogen transport equation is solved first and then the mass fraction of water is obtained. Similarly, for the cathode side, the transport equations are solved for two species, since the third one can be easily obtained from the mass balance equation. These are given in Eqn. (21) and Eqn. (22), respectively.

$$\omega_{H_2O} = 1 - \omega_{H_2} \tag{25}$$

$$\omega_{N_2} = 1 - \omega_{O_2} - \omega_{H_2O} \tag{26}$$

Two phase flow dynamics is coupled with the porous electrode reaction for the PEM fuel cell electrochemical

Please cite this article in press as: Chowdhury MZ, et al., Numerical optimization of channel to land width ratio for PEM fuel cell, International Journal of Hydrogen Energy (2018), https://doi.org/10.1016/j.ijhydene.2017.12.149

Table 2 – Major model parameters.

Parameter	Value
Channel Length (m)	25×10^{-3}
Channel depth (m)	1×10^{-3}
GDL width (m)	410×10^{-6}
Catalyst layer thickness (m)	15×10^{-6}
Membrane thickness (m)	50×10^{-6}
GDL porosity	0.4 [36]
GDL permeability (m^2)	1.0×10^{-12} [36,44]
GDL electric conductivity (S/m)	222 [48]
Inlet H_2 mass fraction (anode)	0.65
Inlet H_2O mass fraction (cathode)	0.05
Inlet oxygen mass fraction (cathode)	0.20
Anode inlet flow velocity (m/s)	0.25
Cathode inlet flow velocity (m/s)	0.625
Anode viscosity (Pa·s)	1.19×10^{-5}
Cathode viscosity (Pa·s)	2.46×10^{-5}
Hydrogen molar mass (kg/mol)	0.002
Nitrogen molar mass (kg/mol)	0.028
Water molar mass (kg/mol)	0.018
Oxygen molar mass (kg/mol)	0.032
H_2–H_2O binary diffusion coefficient (m^2/s)	11.676×10^{-5} [45]
N_2–H_2O binary diffusion coefficient (m^2/s)	3.266×10^{-5} [45]
O_2–N_2 binary diffusion coefficient (m^2/s)	3.044×10^{-5} [45]
O_2–H_2O binary diffusion coefficient (m^2/s)	3.578×10^{-5} [45]
Cell temperature (K)	353
Reference pressure (Pa)	101.325×10^3
Open circuit cell voltage (V)	0.9
Membrane conductivity (S/m)	10 [29]
Anodic transfer coefficient	1 [48]
Cathodic transfer coefficient	1 [48]
Tafel slope, A_c (mV)	−95
Oxygen reference concentration (mol/m^3)	40.88 [36]
Hydrogen reference concentration (mol/m^3)	40.88 [36]
Electrolyte phase volume fraction	0.3
Open volume fraction for gas diffusion in porous electrode	0.3
Permeability of catalyst layers (m^2)	1.0×10^{-12} [46]
Faradays Constant (C/mol)	96,485
Anode ref. Exchange current density (A/m^2)	10^5 [50]
Cathode ref. Exchange current density (A/m^2)	1 [50]

modeling. Since reaction only occurs in the catalyst layer for the single phase condition, the mass generation source terms (R_i) for hydrogen, oxygen and water are defined by using Faraday's Law as follows, respectively [40]:

$$R_{H_2} = -\frac{i_a}{2F}M_{H_2} \quad R_{O_2} = \frac{|i_c|}{4F}M_{O_2} \quad R_{H_2O} = -\frac{|i_c|}{2F}M_{H_2O} \tag{27}$$

where F is Faraday's constant.

Initial and boundary conditions

The boundary and initial conditions for this numerical study are defined [29,40,42] and set as follows:

- The internal boundaries are continuous for all domains
- Symmetric boundary conditions are assigned for the gas diffusion and catalyst layers
- No slip condition is applied for all flow channel walls
- All initial values are set to zero
- Convective flux boundary is applied
- For the inlet and outlet, constrain outer edges are set to zero
- Reference pressure is set to 101,325 Pa
- Inlet flow rates for the anode and cathode are taken as constant
- Electrolyte and electric potentials are set to zero for the cathode while the electrolyte potential is defined as zero for the anode and as open circuit potential for the cathode as initial conditions

Numerical solution technique and selected model parameters

The simulations are carried on a Workstation Computer configuring 12-core, 3.4 GHz AMD Ryzen Processor with 3000 MHz 64 GB RAM. The solution of this study is solved for an approximate time of 146–150 h.

The above mathematical equations for the charge generation and distribution, species flow and mass fraction in the flow channels as well as in the porous media are introduced to the Comsol multi-physics module interface, which employs the finite element approach. The solution is achieved by coupling two reacting flow in porous media and two concentrated species modules for both the anode and cathode interfaces to current distribution interface [36]. The model is solved for the unknown variables of electronic and ionic potentials, species mass fraction, velocity and pressure distributions. The solver based on the finite element technique, is used to solve the governing equations shown in Fig. 2. The stationary nonlinear solver is used since the source terms of the current conservation equation make the problem nonlinear. Furthermore, the convergence behavior of this nonlinear solver is highly sensitive to the initial estimation of the solution.

Validation of the mathematical model

The mathematical model developed is firstly validated with the experimental results reported in our previous experimental study [47] for the two conventional serpentine flow fields (S1 and S2), considering the same operating conditions and other major parameters of the numerical model given in Table 2. The validation results are shown in Fig. 3, where less than 1% error is obtained for both cases, which indicates that the mathematical model agrees well with the experimental study.

Results and discussion

This study considered of a fixed operating voltage of 0.4 V. For the optimization of both the channel and land width, the current density and anode and cathode pressure drop are considered for a comparative study.

Please cite this article in press as: Chowdhury MZ, et al., Numerical optimization of channel to land width ratio for PEM fuel cell, International Journal of Hydrogen Energy (2018), https://doi.org/10.1016/j.ijhydene.2017.12.149

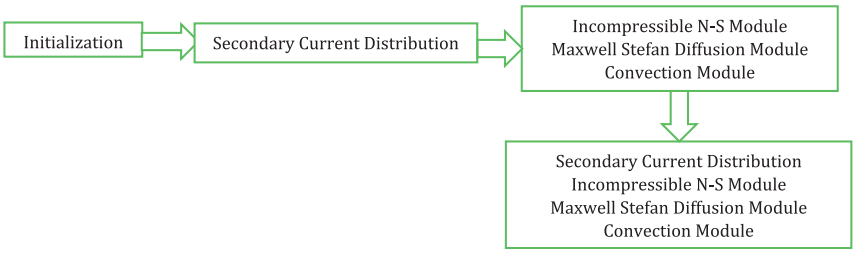

Fig. 2 – Sequence of solver configuration for the numerical model.

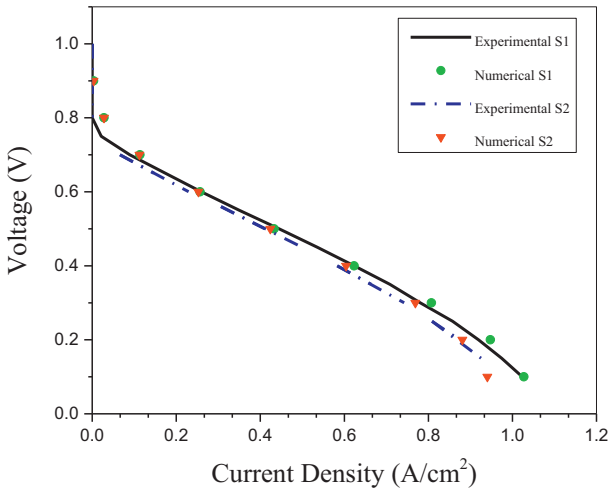

Fig. 3 – Validation of numerical model with the experimental study in Ref. [47].

Effect on current density

The predicted cell current density for different constant land width cases with the variation of channel width are illustrated graphically in Fig. 4. From the predicted results, it can be observed that for the constant land width of 0.25 mm, 0.5 mm and 0.75 mm cases, with the increase of channel width from 0.25 mm to 2.0 mm, the current density decreased linearly. However, for the other constant land width case (1.0 mm, 1.25 mm and 1.5 mm), the current density are at the lower side for the relevant lowest channel width but after that the current density started to increase with the increase of channel width until it reaches a peak value at the channel width of 1.0 mm. Further increase in the channel width beyond 1.0 mm, the current density again started to fall and decreased linearly. Also, it can be noticed that, both the peak and minimum value of the cell current density are predicted for the constant land width of 0.25 mm, where the maximum and minimum value gained for the relevant minimum and maximum channel width respectively.

From the perspective point of constant channel width analyses, variation of the cell current density with the change in land width is graphically exhibited in Fig. 5. In this case also, the maximum and minimum cell current density occurred at the minimum constant channel width for the dimension of minimum and maximum land width respectively. With the increase in constant channel width value, the peak cell current density transforms from the lower land width dimension to the higher land width dimension. Therefore, it can be concluded that the narrow channel dimension results to a better current density [48,49].

From the both perspective data analyses for constant channel and land width, it can be observed that the fluctuation of the cell current density is much higher for the variation in channel width than the land width for their respective land and channel width. From the numerical results, it can be concluded that for the minimum of both channel and land width yields a higher cell current density i.e. both channel and land width dimensions have equal importance for the cell current density.

Effect on pressure drop

The pressure drop for both anode and cathode decrease with the increase in the channel width for different constant land width cases. The anode and cathode pressure drop with channel width for different constant land width are shown in Fig. 6a and b respectively. It can be observed that the anode pressure drop is not that much high compare to the cathode pressure drop. Also variation of both anode and cathode pressure drop for the different constant land width are so small. This can be understand more clearly from Fig. 7a and b, where the anode and cathode pressure drop are varied with the change of land width for different constant channel width respectively. From Figs. 6 and 7, it can be observed that cathode pressure drop is more sensitive than the anode pressure drop. The cathode pressure drop seems to be more significantly high especially lower than the 1.0 mm channel width dimension. On the other hand, variation in land width has almost no effect on the pressure drop for both anode and cathode.

Optimization of channel and land width

For the geometry optimization of channel to land width ratio, the cases of current density and pressure drop have been scrutinized. A suitable channel geometry for PEMFC should have neither high pressure drop nor low current density. High pressure drop is not desired due to the extra pumping work required for higher pressure drop in PEM fuel cell which ultimately reduces the cell efficiency. From the case studies, two points are obvious: (1) land width has little or no effect on pressure drop and (2) the anode pressure drop is negligible compared to the cathode pressure drop. Meanwhile, both channel and land width have noticeable consequences on the

Please cite this article in press as: Chowdhury MZ, et al., Numerical optimization of channel to land width ratio for PEM fuel cell, International Journal of Hydrogen Energy (2018), https://doi.org/10.1016/j.ijhydene.2017.12.149

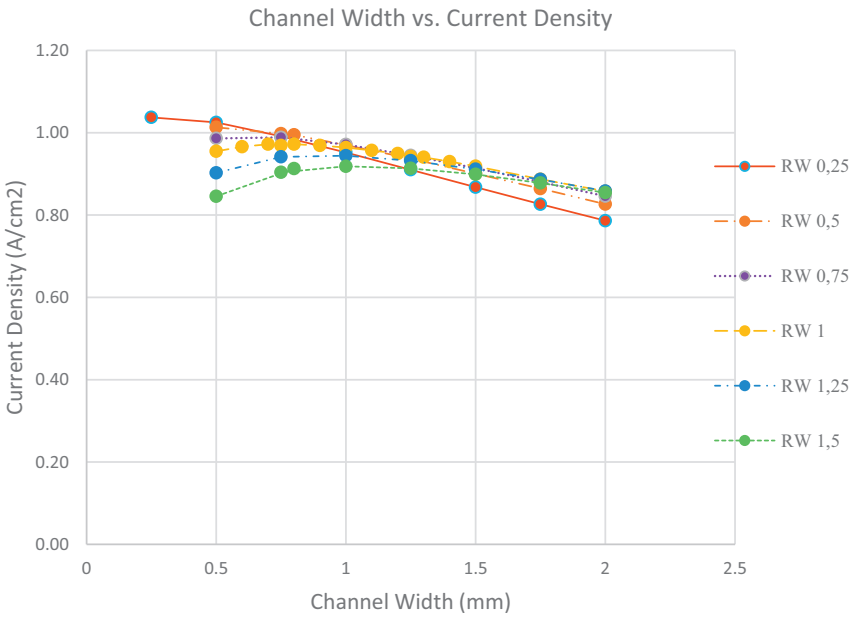

Fig. 4 – Variation in current density for different channel width considering for different constant land width (RW) at 0.4 V.

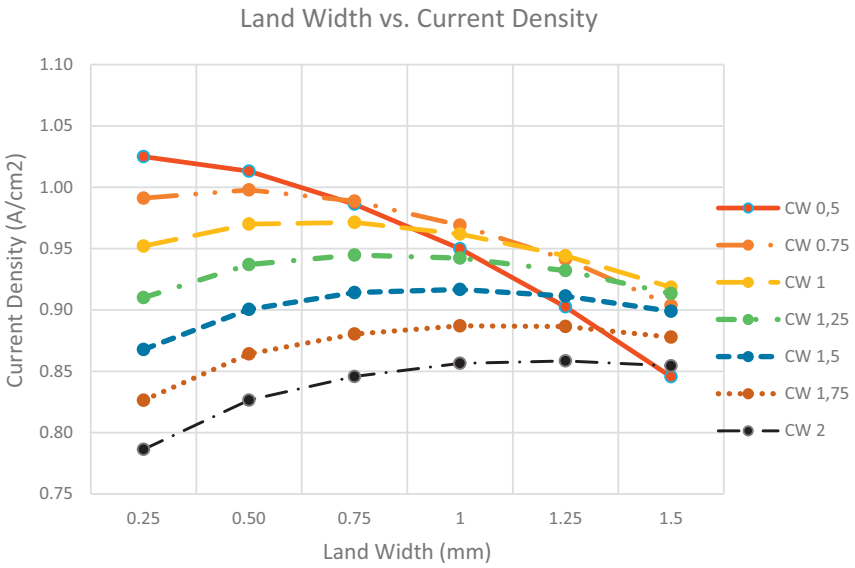

Fig. 5 – Variation in current density for different land width considering for different constant channel width (CW) at 0.4 V.

current density. Contemplating on all of these issues, maximum and minimum cases of pressure drops as well as current density are analyzed from the resulting data for a suitable channel geometry.

The final geometry is selected such that the cell should provide an acceptable current density along with a moderate pressure drop as well as have a compact geometry. The results of the analyses together with the selected dimensions are summarized in Table 3, for the optimization of channel geometry.

The cell current density is higher for the minimum channel and land width dimension [48]. The maximum current density predicted from this study is 1.04 A/cm^2 for the channel to land width of 0.25/0.25. But in this case, high cathode pressure drop occurred which is about 92 Pa for just a 25 mm channel length. On the other hand, if the lower cathode pressure drop is considered from the numerical results, which is as low as 6 Pa for the channel to land width of 2.0/0.25 case and is highly considerable as the channel pressure drop for the suitable geometry. But the corresponding current density for this case is only 0.79 A/cm^2, which is in the lower side for the considered smaller scale geometry length. Also, the channel width of 2.0 mm relating with 0.25 mm land width are not suitable for high contact resistance as it will increase ohmic resistance

Please cite this article in press as: Chowdhury MZ, et al., Numerical optimization of channel to land width ratio for PEM fuel cell, International Journal of Hydrogen Energy (2018), https://doi.org/10.1016/j.ijhydene.2017.12.149

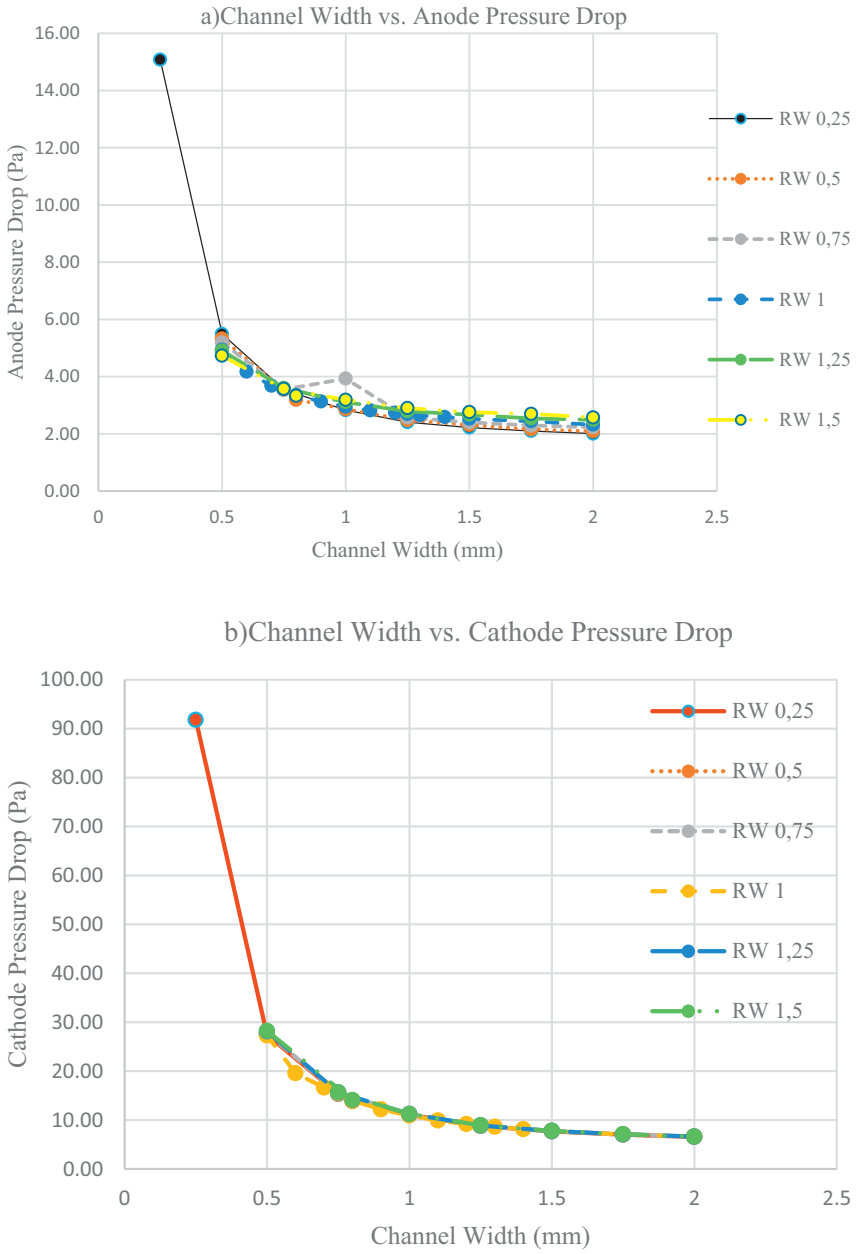

Fig. 6 – Pressure drop for different channel width in accordance with the different constant land width (RW) (a) Anode Pressure Drop (b) Cathode Pressure Drop.

[17]. So further looking into the numerical results, it is observed that, for the of channel width of 1.0 mm and land width of 1.0 mm case, the current density is 0.96 A/cm^2 and the corresponding anode and cathode pressure drop are 3 Pa and 11 Pa respectively, which has the expected cell performance along with considerable pressure drop as well as having a compact channel geometry. Therefore, from the optimization analyses, it is decided that, channel width of 1.0 mm and land width of 1.0 mm are the most suitable dimensions considering the cell current density and pressure drop.

The numerical results of the selected optimized case study's cell current density along with the anode and cathode pressure drop are depicted in Fig. 8 for an operating voltage of 0.4 V. From the numerical result of the considered optimized case, the current density seems to be uniform and current density is higher at the inlet and under the land than the outlet section and the channel width respectively depicted in Fig. 8a. On the other hand, higher pressure distribution existed in the channel inlet section for both anode and cathode channel shown in Fig. 8 (b) and (c). The pressure reduced from the inlet towards the outlet due to the molecular diffusion of

Please cite this article in press as: Chowdhury MZ, et al., Numerical optimization of channel to land width ratio for PEM fuel cell, International Journal of Hydrogen Energy (2018), https://doi.org/10.1016/j.ijhydene.2017.12.149

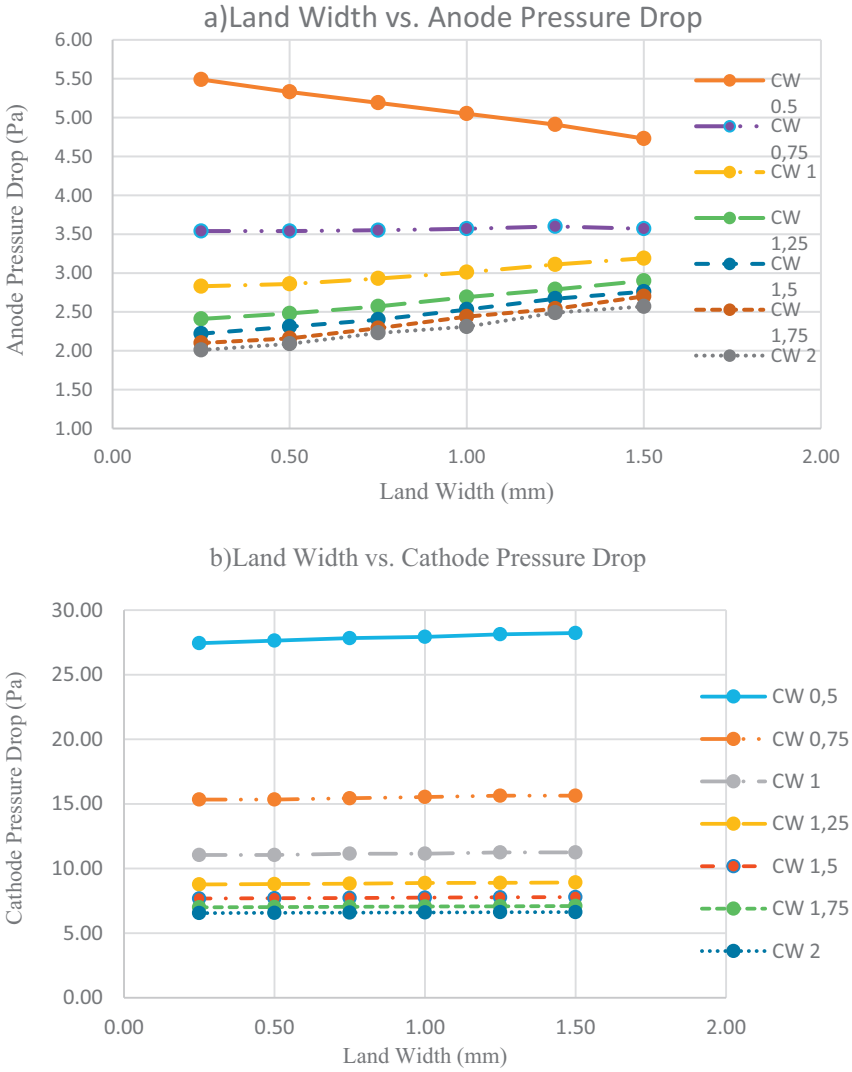

Fig. 7 – Pressure drop for different land width in accordance with the different constant channel width (CW) (a) Anode Pressure Drop (b) Cathode Pressure Drop.

Table 3 – Channel geometry optimization analyses.

Case	Channel to land width mm/mm	Pressure Drop (Anode/Cathode) Pa/Pa	Current Density A/cm^2	Summary
Max. Current Density	0.25/0.25	15/92	1.04	Highest current density and higher cathode pressure drop
Max. Pressure Drop	0.2/0.8	16/137	0.84	Current density in lower side with highest cathode pressure drop
Min. Current Density and Pressure Drop	2.0/0.25	2/6	0.79	Lowest current density with lowest pressure drop
Selected Case	1.0/1.0	3/11	0.96	Considerable pressure drop with high current density

gas mixture and frictional loss at the channel boundary sections. The cathode pressure drop is much higher comparative to the anode channel mainly due to the reason of more complex gas mixture in the cathode channel. It can be also due to the produced water at the cathode channel which adds a new stream in the cathode channel and the cathode flow stream faced more resistance as it tries to remove the produced water from the cathode channel which results in a reduced momentum of the cathode stream resulting in a higher pressure drop at the cathode channel.

Please cite this article in press as: Chowdhury MZ, et al., Numerical optimization of channel to land width ratio for PEM fuel cell, International Journal of Hydrogen Energy (2018), https://doi.org/10.1016/j.ijhydene.2017.12.149

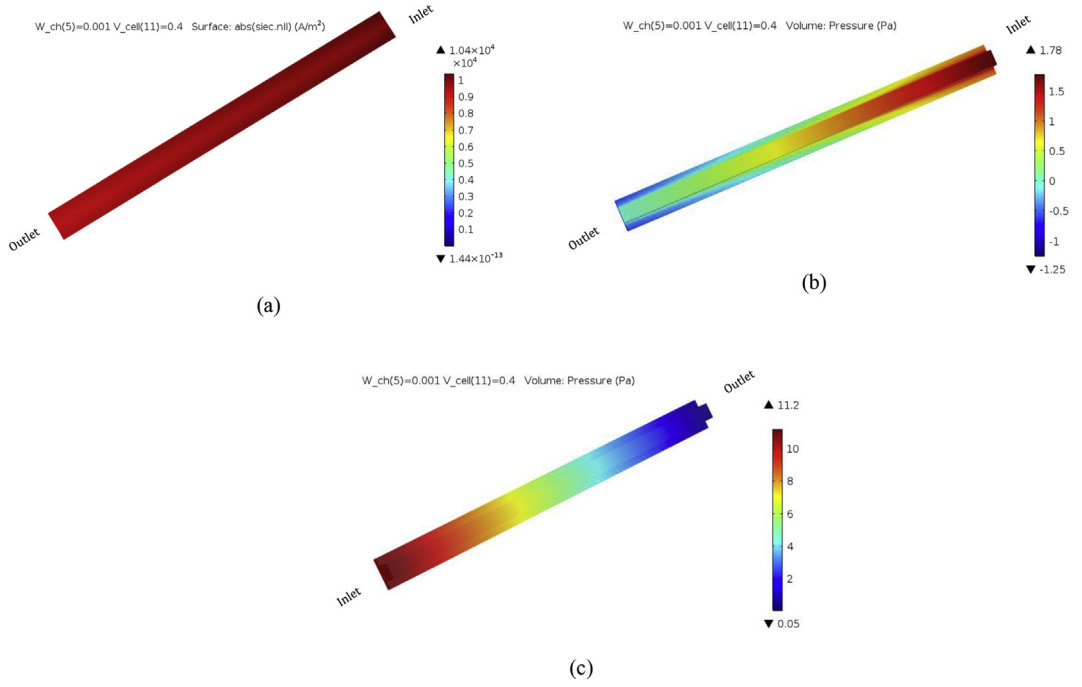

Fig. 8 – The selected optimized case study's (a) surface current density (b) anode pressure drop (c) cathode pressure drop.

Conclusions

The numerical analyses for the optimization of channel and land width in PEM fuel cell were investigated for a total of staggering 73 case studies. From the predicted results of the current density and channel pressure drop behavior were more easily understood with better reliability. The results predicted that the effect of channel width has more impact on pressure drop than land width. The minimum the channel width, the maximum the pressure drop is. On the other hand, land width has little or negligible effect on the pressure drop. Beside this, the study revealed that the anode pressure is not significant compared to the cathode pressure drop. Meanwhile, both channel and land width have equal importance on the cell current density. The minimum dimension of the channel and land width predicted to have a better cell current density. However, at the minimum channel dimension, the pressure drop is too high which will reduce the overall cell efficiency. Due to this reason, an optimization analyses were carried out from the large number of data of the considered case studies, where it was found that the channel to land width of 1.0 mm/1.0 mm would provide the best cell performance having a cell current density of 0.96 A/cm^2 and 3 Pa/11 Pa for anode/cathode pressure drop.

Acknowledgment

This research supported by Nigde Omer Halisdemir University Scientific Research Projects Coordination Unit under a project number of FEB2016/31-YULTEP is gratefully acknowledged.

REFERENCES

[1] Midilli A. Green hydrogen energy system: a policy on reducing petroleum-based global unrest. Int J Glob Warming 2016;10:354–70.
[2] Alaswad A, Baroutaji A, Achour H, Carton J, Al-Makky A, Olabi AG. Developments in fuel cell technologies in the transport sector. Int J Hydrogen Energy 2016;41:16499–508.
[3] van Dokkum J, Dasinger A. Meeting the challenges in the transport sector. J Power Sources 2008;181:378–81.
[4] Li X, Sabir I. Review of bipolar plates in PEM fuel cells: flow field designs. Int J Hydrogen Energy 2005;30:359–71.
[5] Ozden E, Tari I. Proton exchange membrane fuel cell degradation: a parametric analysis using Computational Fluid Dynamics. J Power Sources 2016;304:64–73.
[6] Dawes JE, Hanspal NS, Family OA, Turan A. Three dimensional CFD modelling of PEM fuel cells: an investigation into the effects of water flooding. Chem Eng Sci 2009;64:2781–94.
[7] Manso AP, Marzo FF, Mujika MG, Barranco J, Lorenzo A. Numerical analysis of the influence of the channel cross-section aspect ratio on the performance of a PEM fuel cell with serpentine flow field design. Int J Hydrogen Energy 2011;36:6795–808.
[8] Grigoriev SA, Kalinnikov AA, Kuleshov NV, Millet P. Numerical optimization of bipolar plates and gas diffusion electrodes for PBI-based PEM fuel cells. Int J Hydrogen Energy 2013;38:8557–67.
[9] Kreesaeng S, Chalermsinsuwan B, Piumsomboon P. Effect of channel designs on open-cathode PEM fuel cell performance: a computational study. Energy Procedia 2015;79:733–45.
[10] Rostami L, Nejad PMG, Vatani A. A numerical investigation of serpentine flow channel with different bend sizes in polymer electrolyte membrane fuel cells. Energy 2016;97:400–10.
[11] Salah YB, Tabe Y, Chikahisa T. Two phase flow simulation in a channel of a polymer electrolyte membrane fuel cell using

Please cite this article in press as: Chowdhury MZ, et al., Numerical optimization of channel to land width ratio for PEM fuel cell, International Journal of Hydrogen Energy (2018), https://doi.org/10.1016/j.ijhydene.2017.12.149

the lattice Boltzmann method. J Power Sources 2012;199:85–93.
[12] Lorenzini-Gutierrez D, Kandlikar SG, Hernandez-Guerrero A, Elizalde-Blancas F. Residence time of water film and slug flow features in fuel cell gas channels and their effect on instantaneous area coverage ratio. J Power Sources 2015;279:567–80.
[13] Xing L, Cai Q, Liu X, Liu C, Scott K, Yan Y. Anode partial flooding modelling of proton exchange membrane fuel cells: ooptimisation of electrode properties and channel geometries. Chem Eng Sci 2016;146:88–103.
[14] Akhtar N, Qureshi A, Scholta J, Hartnig C, Messerschmidt M, Lehnert W. Investigation of water droplet kinetics and optimization of channel geometry for PEM fuel cell cathodes. Int J Hydrogen Energy 2009;34:3104–11.
[15] Higier A, Liu H. Optimization of PEM fuel cell flow field via local current density measurement. Int J Hydrogen Energy 2010;35:2144–50.
[16] Berning T, Djilali N. Three-dimensional computational analysis of transport phenomena in a PEM fuel cell—a parametric study. J Power Sources 2003;124:440–52.
[17] Akbari MH, Rismanchi B. Numerical investigation of flow field configuration and contact resistance for PEM fuel cell performance. Renew Energy 2008;33:1775–83.
[18] Al-Baghdadi MARS, Al-Janabi HAKS. Parametric and optimization study of a PEM fuel cell performance using three-dimensional computational fluid dynamics model. Renew Energy 2007;32:1077–101.
[19] Yu LJ, Ren GP, Qin MJ, Jiang XM. Transport mechanisms and performance simulations of a PEM fuel cell with interdigitated flow field. Renew Energy 2009;34:530–43.
[20] Goebel SG. Impact of land width and channel span on fuel cell performance. J Power Sources 2011;196:7550–4.
[21] Hsieh SS, Chu KM. Channel and rib geometric scale effects of flow field plates on the performance and transient thermal behavior of a micro-PEM fuel cell. J Power Sources 2007;173:222–32.
[22] Wang XD, Yan WM, Duan YY, Weng FB, Jung GB, Lee CY. Numerical study on channel size effect for proton exchange membrane fuel cell with serpentine flow field. Energy Convers Manag 2010;51:959–68.
[23] Jahnke T. Performance and degradation of proton exchange membrane fuel cells: state of the art in modeling from atomistic to system scale. J Power Sources 2016;304:207–33.
[24] Mukherjee PP, Wang C-Y, Kang Q. Mesoscopic modeling of two-phase behavior and flooding phenomena in polymer electrolyte fuel cells. Electrochim Acta 2009;54(27):6861–75.
[25] Siegel C. Review of computational heat and mass transfer modeling in polymerelectrolyte-membrane (PEM) fuel cells. Energy 2008;33(9):1331–52.
[26] Andersson M, Beale SB, Espinoza M, Wu Z, Lehnert W. A review of cell-scale multiphase flow modeling, including water management, in polymer electrolyte fuel cells. Appl Energy 2016;180:757–78.
[27] Yang WJ, Wang HY, Kim YB. Channel geometry optimization using a 2D fuel cell model and its verification for a polymer electrolyte membrane fuel cell. Int J Hydrogen Energy 2014;39:9430–9.
[28] Xing L, Cai Q, Xu C, Liu C, Scott K, Yan Y. Numerical study of the effect of relative humidity and stoichiometric flow ratio on PEM (proton exchange membrane) fuel cell performance with various channel lengths: an anode partial flooding modeling. Energy 2016;106:631–45.
[29] Sezgin B, Caglayan DG, Devrim Y, Steenberg T, Eroglu I. Modeling and sensitivity analysis of high temperature PEM fuel cells by using Comsol Multiphysics. Int J Hydrogen Energy 2016;41:10001–9.
[30] Caglayan DG, Sezgin B, Devrim Y, Eroglu I. Three-dimensional modeling of a high temperature polymer electrolyte membrane fuel cell at different operation temperatures. Int J Hydrogen Energy 2016;41:10060–70.
[31] Lobato J, Canizares P, Rodrigo MA, Pinar FJ. Three dimensional modeling of a 50 cm2 high temperature PEM fuel cell, study of the flow channel geometry influence. Int J Hydrogen Energy 2010;35:5510–20.
[32] Haase S, Mueller S. Pressure distribution method for ex-situ evaluation of flow distribution in polymer electrolyte membrane fuel cells. J Power Sources 2015;280:612–20.
[33] Verma A, Pitchumani R. Influence of membrane properties on the transient behavior of polymer electrolyte fuel cells. J Power Sources 2014;268:733–43.
[34] Ismail MS, Hughes KJ, Ingham DB, Ma L, Pourkashanian M. Effects of anisotropic permeability and electrical conductivity of gas diffusion layers on the performance of proton exchange membrane fuel cells. Appl Energy 2012;95:50–63.
[35] Cooper NJ, Santamaria AD, Becton MK, Park JW. Investigation of the performance improvement in decreasing aspect ratio interdigitated flow field PEMFCs. Energy Convers Manag 2017;136:307–17.
[36] Bao C, Bessler WG. Two-dimensional modeling of a polymer electrolyte membrane fuel cell with long flow channel. Part I. Model development. J Power Sources 2015;275:922–34.
[37] Khan MA. Multiphysics modelling of PEM fuel cells: with reacting transport phenomena at micro and macroscales. Lund: Lund University; 2011.
[38] Ghanbarian A, Kermani MJ. Enhancement of PEM fuel cell performance by flow channel indentation. Energy Convers Manag 2016;110:356–66.
[39] Ramiar A, Mahmoudi AH, Esmaili Q, Abdollahzadeh M. Influence of cathode flow pulsation on performance of proton exchange membrane fuel cell with interdigitated gas distributors. Energy 2016;94:206–17.
[40] Wu H. A review of recent development: transport and performance modeling of PEM fuel cells. Appl Energy 2016;165:81–106.
[41] Ferreira RB, Falcao DS, Oliveira VB, Pinto AMFR. Numerical simulations of two-phase flow in proton exchange membrane fuel cells using the volume of fluid method – a review. J Power Sources 2015;277:329–42.
[42] Xing L, Du S, Chen R, Mamlouk M, Scott K. Anode partial flooding modelling of proton exchange membrane fuel cells: model development and validation. Energy 2016;96:80–95.
[43] Perng SW, Wu HW. Non-isothermal transport phenomenon and cell performance of a cathodic PEM fuel cell with a baffle plate in a tapered channel. Appl Energy 2011;88:52–67.
[44] Khazaee I, Sabadbafan H. Effect of humidity content and direction of the flow of reactant gases on water management in the 4-serpentine and 1-serpentine flow channel in a PEM (proton exchange membrane) fuel cell. Energy 2016;101:252–65.
[45] Osanloo B, Mohammadi-Ahmar A, Solati A. A numerical analysis on the effect of different architectures of membrane, CL and GDL layers on the power and reactant transportation in the square tubular PEMFC. Int J Hydrogen Energy 2016;41:10844–53.
[46] Salva JA, Iranzo A, Rosa F, Tapia E. Validation of cell voltage and water content in a PEM (polymer electrolyte membrane) fuel cell model using neutron imaging for different operating conditions. Energy 2016;101:100–12.

Please cite this article in press as: Chowdhury MZ, et al., Numerical optimization of channel to land width ratio for PEM fuel cell, International Journal of Hydrogen Energy (2018), https://doi.org/10.1016/j.ijhydene.2017.12.149

[47] Chowdhury MZ, Akansu YE. Novel convergent-divergent serpentine flow fields effect on PEM fuel cell performance. Int J Hydrogen Energy 2017;42:25686–94.
[48] Muthukumar M, Karthikeyan P, Vairavel M, Loganathan C, Praveenkumar S, Senthil Kumar AP. Numerical studies on PEM fuel cell with different landing to channel width of flow channel. Procedia Eng 2014;97:1534–42.
[49] Bilgili M, Bosomoiu M, Tsotridis G. Gas flow field with obstacles for PEM fuel cells at different operating conditions. Int J Hydrogen Energy 2015;40:2303–11.
[50] Ionescu V. Finite element method modelling of a high temperature PEM fuel cell. Rom Journ Phys 2014;59:285–94.

Please cite this article in press as: Chowdhury MZ, et al., Numerical optimization of channel to land width ratio for PEM fuel cell, International Journal of Hydrogen Energy (2018), https://doi.org/10.1016/j.ijhydene.2017.12.149